WIRELESS METAMATERIAL-INSPIRED ROTATION SENSORS

A THESIS SUBMITTED TO
THE GRADUATE SCHOOL OF ENGINEERING AND SCIENCE
OF BILKENT UNIVERSITY
IN PARTIAL FULFILLMENT OF THE REQUIREMENTS FOR
THE DEGREE OF
MASTER OF SCIENCE
IN
ELECTRICAL AND ELECTRONICS ENGINEERING

By
Ali Maleki Gargari
June 2017

Wireless Metamaterial-Inspired Rotation Sensors
By Ali Maleki Gargari
June 2017

We certify that we have read this thesis and that in our opinion it is fully adequate, in scope and in quality, as a thesis for the degree of Master of Science.

Vakur Behçet Ertürk (Advisor)

Hilmi Volkan Demir (Co-Advisor)

Ayhan Altıntaş

Özgür Kurç

Approved for the Graduate School of Engineering and Science:

Ezhan Karaşan
Director of the Graduate School

ABSTRACT

WIRELESS METAMATERIAL-INSPIRED ROTATION SENSORS

Ali Maleki Gargari
M.S. in Electrical and Electronics Engineering
Advisor: Vakur Behçet Ertürk
Co-Advisor: Hilmi Volkan Demir
June 2017

Recently steel construction structures have been attracting increasingly more attention due to the speed and ease of their construction. However, to detect potential damages in these structures, long-term and cost-effective health monitoring solutions are required. A rotation-based bending movement, which typically occurs in the load carrying elements of these structures (such as beams), is an example of the aforementioned potential damage. In this thesis, for measuring small bending rotations ($10^{-4} \sim 10^{-5}$ radians) in the structures made of materials such as steel, a novel wireless rotation sensing system with a high level of sensitivity and resolution is proposed and demonstrated. This system consists of two elements: an interrogating antenna and an inter-digital double-layer sensor. The proposed sensing system operates based on the principle of near-field coupling between the antenna and the sensor. Briefly, by rotating one layer with respect to the other, the electromagnetic coupling between the layers changes and the resonance frequency is consequently shifted. This frequency shift can be recorded by tracking the resonance dips in the S_{11} response of the antenna. In the thesis work, various experiments were systematically performed to characterize the sensing system. A high rotation resolution of 20 μ-radians, an excellent sensitivity level of 28 MHz/degree, and a large dynamic range extending over 40° were measured. Furthermore, the validity of measurement results was verified by using full-wave electromagnetics simulator and applying digital image correlation (DIC) method for 2D measurements.

Keywords: Wireless passive sensor, rotation sensor, metamaterial-inspired sensor.

ÖZET

KABLOSUZ METAMALZEMEDEN İLHAM ALINAN DÖNÜŞ ALGILAYICILARI

Ali Maleki Gargari
Elektrik ve Elektronik Mühendisliği, Yüksek Lisans
Tez Danışmanı: Vakur Behçet Ertürk
Tez Eş-Danışmanı: Hilmi Volkan Demir
Haziran 2017

Son yıllarda, yapısal taşıyıcı sistemi çelik olan yapılar, inşaat hızı ve kolaylığı gibi sebeplerle daha fazla dikkat çekmektedir. Ancak bu yapılardaki olası hasarların saptanması için uzun vadeli ve ucuz yapısal sağlık izleme çözümlerine ihtiyaç vardır. Bu yapıların yük taşıyan elemanlarında (kiriş gibi) oluşan dönme tabanlı eğilme hareketi yukarıda bahsedilen potansiyel hasarlara bir örnektir. Bu tezde çelik ve benzeri yapılardaki eğilme davranışı kaynaklı çok küçük dönme miktarlarını ($10^{-4} \sim 10^{-5}$ radyan) ölçebilecek yüksek çözünürlük ve hassasiyete sahip yeni kablosuz bir algılama sistemi önerilmekte ve gösterilmektedir. Bu sistem iki elemandan oluşmaktadır: sorgulamayı yapan bir anten ve parmak arası yapısında iki katmandan oluşan bir algılayıcı. Bu sistem anten ve algılayıcının yakın alan bağlaşması prensibini baz alarak çalışmaktadır. Kısaca, algılayıcının katmanlarından birini diğerine göre döndürerek, katmanlar arasındaki elektromanyetik bağlaşma değişmekte ve bunun sonucunda da rezonans frekansı kaymaktadır. Bu frekans değişimi, antenin S_{11} cevabında görünen resonans çukurlarını takip ederek kaydedilir. Bu tezde, önerilen algılama sistemini nitelemek amacı ile sistematik olarak farklı deneyler gerçekleştirilmiştir. 20 mikro-radyan mertebesinde yüksek bir dönme çözünürlüğü, 28 MHz/derecelik bir harika hassasiyet ve 40 derece civarında genis bir dinamik menzil elde edilmiştir. İlaveten, ölçüm sonuçlarının geçerliliği, tam dalga elektromanyetik benzetim programları ve iki boyutlu ölçümler için dijital resim korelasyon metodu ile doğrulanmıştır.

Anahtar sözcükler: Kablosuz pasif algılayıcı, dönüş algılayıcı, metamalzemeden ilhamlı algılayıcı.

Acknowledgement

At first, I would like to express my sincere gratitude and respect to Prof. Vakur Behçet Ertürk and Prof. Hilmi Volkan Demir who have supervised me during my master studies at Bilkent University. Without a doubt, their endless support, encouragement, priceless guidances, and helpful suggestions have played main roles in success during my graduate study. Secondly, I would like to especially thank Prof. Özgür Kurç and Prof. Ayhan Altintaş for not only allocating their time to evaluate my work and providing me with inestimable comments to make this thesis work stronger, but also their generous support during my research and studies.

I would like to thank Demir group members Emre Ünal and Burak Özbey, and Utku Albostan for the friendly environment they provided, which was perfect for learning. Also, I am thankful to my friends Bahram, Kamal, Sina, Farzan, Alireza, Daryoush, Meysam, Mohammadreza, and Hossein, who provided warm company and scientific arguments and were like a family all these years.

At the end, I would like to dedicate this thesis to my mother, father, and sister. Their spiritual support and love are undeniable facts that have survived me in every difficulty. I could not have imagined a better upbringing if they were not always there for me.

Contents

List of Figures

List of Tables

Chapter 1

Introduction

1.1 Motivation and Objectives

In recent years, steel construction structures have increasingly become popular all around the world due to the advantages they bring in the speed and ease of construction. In time, load-carrying elements such as beams employed in these structures are subject to a bending movement (in the form of a displacement along the load axis, and in the form of rotation perpendicular to the load axis). These movements occur in the elastic deformation region (i.e., reversible damage region). By measuring the amount of rotation along the beam length, it is possible to understand the force, stress, displacement, and strain building up on the beam. Thus, critical information regarding the structural health monitoring (SHM) and inspection of the beam can be acquired. This bending based rotation movement takes place at very small angles ($10^{-4} \sim 10^{-5}$ radians), and hence, their detection requires a system with high precision in terms of sensitivity and resolution. To the best of our knowledge, there is no developed wireless technology that employs passive microwave devices for the telemetric measurement of bending-based deformations with such high sensitivity.

In this thesis, a metamaterial-inspired passive wireless rotation sensing system for the measurement of elastic-region bending in materials such as steel is proposed and demonstrated. The system can be employed in bending elements fabricated from other elastic materials, composites, plastic, and rubbers as well. The sensor is designed particularly to manifest a high level of resolution and sensitivity in capturing very slight angular deviations. The proposed sensor is based on the principle of near-field coupling between the antenna and the sensor. This feature enhances the key parameters such as sensitivity, resolution and signal-to-noise ratio.

1.2 Thesis Outline

In Chapter 2, literature is reviewed and a comprehensive discussion on metamaterials, metamaterial-inspired structures, and rotation sensors is presented. In Chapter 3, characterization parameters of a sensor such as sensitivity and resolution are defined and its design procedure is explained. Then, architecture of the sensor is discussed and its operating principle is also explained. In Chapter 4, by utilizing parameters such as sensitivity, dynamic range, monitoring distance, and resolution, various experiments are introduced and investigated. Furthermore, the validity of measurement results has been verified by using a full-wave electromagnetics simulator as well as applying digital image correlation (DIC) method for 2D measurements. Finally in Chapter 5, a brief summary of results and future steps is described.

Chapter 2

Literature Review and Theoretical Background

Metamaterials (MMs), which are described as artificially engineered materials, can have negative permittivity and/or negative effective permeability. Initially in 1968, Veselago theoretically introduced the left-handed materials (LHMs) that can have both negative permittivity and permeability. In the LHMs, the directions of the propagation of phase velocity and group velocity are in the opposite directions. Periodic arrangement of thin wires can provide negative permittivity. Also, in order to achieve negative permeability, split ring resonators (SRRs) were proposed by Pendry *et al.* in 1996 [1]. Then, arrays of periodic SRRs and thin wires called as composite metamaterials (CMMs) were initially tested by Smith *at al.* [2, 3] and a wide range of applications of MMs have been introduced. Periodic arrangements of SRRs have numerous applications in MMs. However, deploying a single unit of SRR offers other advantages. Marquees *et al.* [4] suggested the idea of single SRR as a resonator and modeled it with an equivalent LC circuit. Until now, different types of SRRs have been designed and proposed in literature as subwavelength resonators; for instance, complementary split ring resonators (CSRR) [5, 6], closed ring resonators (CRR) [7], broadside coupled split resonators (BCSRR) [8], multi split ring resonator (MSRR) [9], and comb-like split ring resonators [9, 10].

In metamaterial-inspired (MMI) structures, instead of employing bulk medium such as an array of MMs, only a single MM unit cell is used [11]. In sensing applications of these structures, any variation in the quantity of interest can be modeled and represented by a change in resonance frequency and/or loss in the frequency response of the sensor [12,13]. Based on this idea, different sensing problems are solved and various types of sensors such as biosensors [14–16], strain sensors [17–20], and displacement sensors [21–24] are introduced. Although MMI based rotation sensors have also been previously reported [25–31], many of these sensing systems are passive and wired, and they are mainly focused on dynamic range rather than sensitivity and resolution. However, bending that occurs in industrial materials (i.e., beams) is in μ-radian scale, and the resolution level of such sensors is typically not sufficient for measuring very small rotations.

For example, a passive MMI rotation sensor was introduced in [25] based on the symmetry properties of the SRRs. In this sensor, a circular SRR was etched in the backside of the substrate and the slit of the rings was aligned with the symmetry plane of the coplanar waveguide (CPW). By breaking this alignment, the resonance frequency of the SRR was excited and a notch in S_{21} response of the CPW was observed. The deviation from symmetric state yielded in a major variation of the notch magnitude and a very small shift in the notch frequency. Furthermore, tracking the variations in amplitude was considered to facilitate its application in velocity sensors. Therefore, the amplitude of the frequency response (notch depths) was chosen as an electrical variable to measure the angular displacement. In principle, various alignment, position, displacement, velocity, and rotation sensor can be designed based on this concept, but all of them would be wired.

In [26,27], a microstrip line and a CPW were loaded with an electric-LC (ELC) resonator (instead of SRRs) to be used as a passive rotation sensor, and its dynamic range was increased up to 90°. The ELC resonator was etched separately in a circular external substrate. Then, the external part was attached to a step motor and fixed within a short distance over the transmission line for sensing the rotation and angular velocity. Moreover, the line pair was modified in a circular

shape to improve the linearity. Again, by rotating the ELC resonator and deviating from the symmetric state, the magnitude of notch depths were shifted. Still, there was a small undesirable shift in the notch frequency of these sensors. Despite their drawbacks, two different applications of the above mentioned rotation sensors have been recently reported in [29] for implementing the spectral signature barcode and in [28] for a precise orientation control in space vehicles (satellites). Similarly, a horn-shaped SRR coupled to CPW was reported in [30]. This passive sensor allows for a precisely fixed resonance frequency and improved linearity by adjusting the length of the SRR's slit. However, the dynamic range was limited to 8°.

All of the aforementioned MMI passive rotation sensors operate based on tracking the shift in the amplitude of the resonance frequency. In contrast, another wired metamaterial-inspired rotation sensor was introduced in [31], which tracks the shift in resonance frequency. In this rotation sensor, a circular shape microstrip transmission line was coupled to two U-shaped resonators that are stacked on top of each other. By rotating the top resonator over the bottom resonator, the overlapping area between the resonators was increased, which yields stronger coupling and larger shift in operating frequency. The dynamic range of this sensor was around 180°.

However, there is also another family of rotation sensors that are active and can be wired or wireless. According to Sun *et al.* [32], a microwave micro electro mechanical system (MEMS) high-speed angular sensor was developed using the multi-user MEMS processes (MUMPs). This sensors was capable of wirelessly measuring the velocity within speed range of 180 rpm to around 1000 rpm. A commercial RF transmitter was integrated with this sensor to detect the signal. In [33], a chirped fiber grating rotation sensor was introduced, which was wired and utilized active elements. This sensor operates based on the shift of the reflective wavelength peak, and measures the rotor's angle in random directions with a full 360° shaft.

In addition, surface acoustic wave (SAW) rotation sensors are also active and can be wired or operated wirelessly [34, 35]. In most of the SAW sensors, an

oscillating electric field creates a mechanical wave. This wave propagates through or on the surface of the material, and any variation in the properties of the propagation path changes the velocity and/or the amplitude of the wave. This variation can be read out by monitoring the frequency response of the sensor. Furthermore, other active rotation sensors such as coupled lasers rotation sensor (CLARS) [36], optical fiber rotation sensor [37], and microwave gyroscope [38] exploit Sagnac effect to measure the rotation. Sagnac effect creates an additional phase shift by propagating an electromagnetic wave along a circular path in a rotating medium.

Despite acceptable performance of the aforementioned rotation sensors in specified applications, they are not appropriate to be utilized in SHM, since they are not simultaneously passive and wireless. Accordingly, featuring high levels of sensitivity and resolution are significantly more important than the dynamic range for measuring the small rotation-based bendings. Therefore, to address this need, passive wireless rotation sensors with submilliradian level of resolution were investigated in this thesis work.

Chapter 3

Modeling and Design

High sensitivity, resolution, and linearity are explicit figures-of-merit of a sensor. This thesis aims to design a wireless passive sensor with high levels of sensitivity and resolution. MMIs are considered as an appropriate choice to design passive sensors. Fabricating the MMI structures over a two-layer circular-shaped substrate provides a sensor that can convert the mechanical rotation into a measurable electrical parameter such as amplitude and frequency of the resonance. Then, an antenna can be used to wirelessly track the measurable electrical parameter. Furthermore, the resonance frequency of the comb-like SRRs is very sensitive to variations in geometrical parameters including the number of their teeth. In order to design a rotation sensor with high levels of sensitivity and resolution, comb-like SRRs can be reformed in circular shape and etched over a two-layer circular-shaped substrate. In general, two different configurations can be used for circular-shaped comb-like SRRs, namely, interdigital and overlapping structures. In the interdigital structure, the separable parts of the comb-like structure move interdigitally with respect to each other. On the other hand, in the overlapping structure, the separable parts move over each other.

In the thesis, two candidate designs were developed based on the interdigital and overlapping structures to achieve aforementioned figures-of-merit. In Section 3.1, architecture of the proposed sensing system is discussed in detail and in Section 3.2, its design procedure is explained.

3.1 Sensing System Architecture and Design

3.1.1 Sensor Part

In this work, we use specifically two different configurations that are inspired from SRRs. The design goal of each configuration is to achieve high sensitivity. These structures are called overlapping and interdigital configuration. Each configuration has two metallic layers and two dielectric layers. The cross-sectional and top views of both the overlapping and interdigital structures are depicted in Figs. 3.1 to 3.4. The arrangement of the layers follows the order of metal, dielectric, metal, and dielectric (MDMD) for the overlapping structure and dielectric, metal, metal, and dielectric (DMMD) for the interdigital structure. The metal layers are in the form of two quarter-ring comb-like configuration with four fingers, $N = 4$. In MDMD structure, metallic layers are separated with a dielectric layer in the middle and in DMMD structure, metallic layers are facing each other.

Each sensor is composed of two dielectric substrates (bottom dielectric and top dielectric) with two interdigital or overlapped metal layers. The thickness of each metal layer is $h_m = 18$ μm. The dielectric substrate is FR-4 with a relative permittivity of 4.3 and a height of $h_d = 1.5$ mm, while the radius of the overall structure is $R = 16.3$ mm. Top and bottom metallic layers are electrically connected to each other in the middle via a metallic mandrel in a diameter of $D_0 = 1$ mm and a height of $H_0 = 4$ mm. In MDMD configuration, the finger width is W, and the gap between fingers is G. On the other hand, in DMMD configuration, the finger widths for the top and bottom quarter-ring comb-like configuration are denoted with W and G, respectively. G_d and G_a are only

considered in DMMD configuration as horizontal and vertical gaps between the fingers. The distance between the fingers in top view of the DMMD sensor are $G + 2 \times G_d$ and $W + 2 \times G_d$, respectively, with $G_d = 0.1$ mm introduced as an additional offset to avoid possible shortcircuiting of the top and metal layers in the case that $G_a = 0.2$ mm (i.e., to guarantee an inter-digital configuration between the metal layers) is not sufficient. Values of G, W, R, and N are locally optimized to achieve the maximum sensitivity, and the process of optimization is extensively explained in Section 3.2.

By considering the top view of the MDMD configuration and rotating one layer with respect to the other one, the overlapping area between the metallic layers is increased or decreased. However, in DMMD configuration, if one layer is rotated with respect to the other one, the metallic layers move interdigitally inside each other. Figs. 3.5 and 3.6 display different rotation positions of MDMD and DMMD configurations, respectively.

The operating principles of both configurations are quite similar to each other. By rotating one layer with respect to the other one, the interdigital area (for DMMD configuration) or the overlapped area (for MDMD configuration) between metallic layers increase (or decrease). Then, the coupling between the layers becomes stronger (or weaker), which changes the equivalent LC (more dominantly C) of the structure and shifts the resulting resonance frequency down (or up).

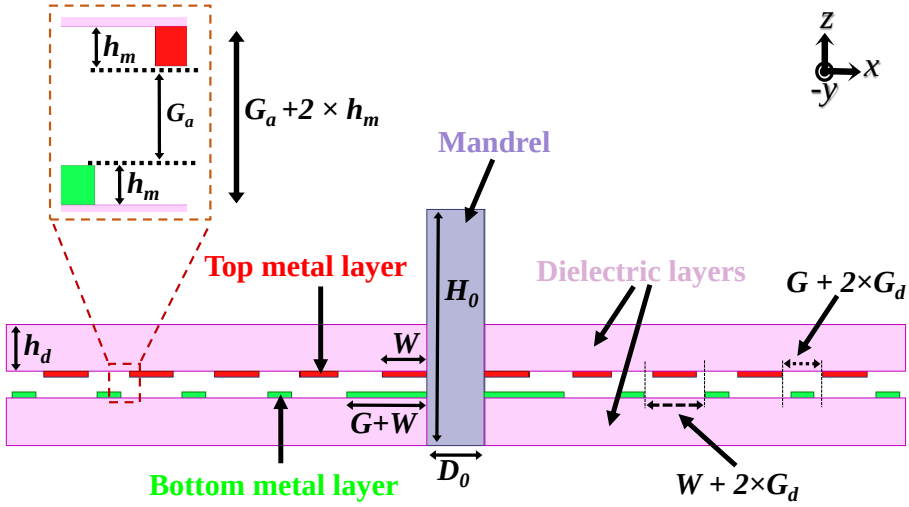

Figure 3.1. Cross-sectional view of the interdigital configuration at the rotation angle of θ=20°, which corresponds to the DMMD arrangement of layers.

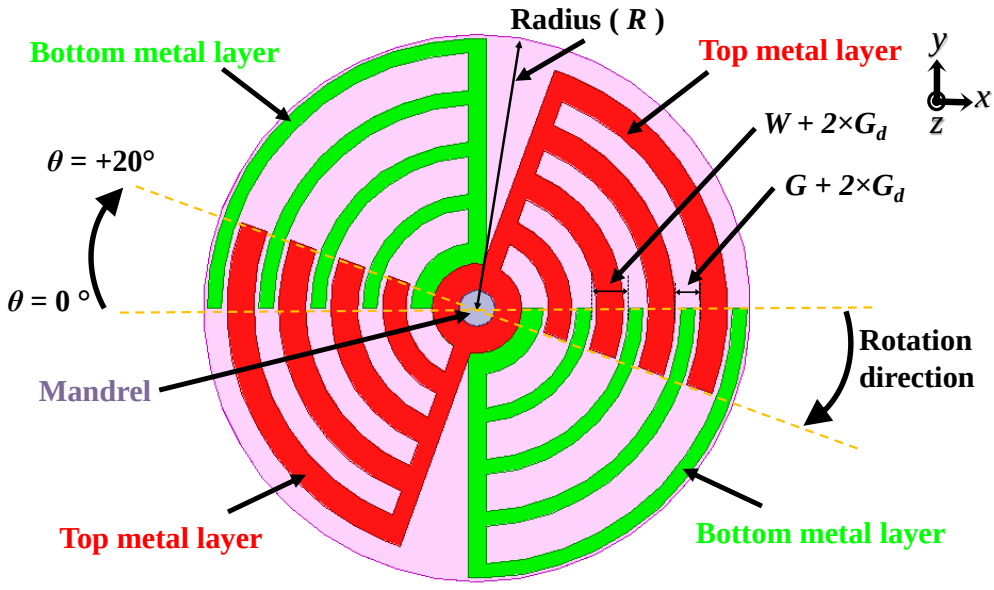

Figure 3.2. Top view of the interdigital configuration at the rotation angle of θ=20°, which corresponds to the DMMD arrangement of layers.

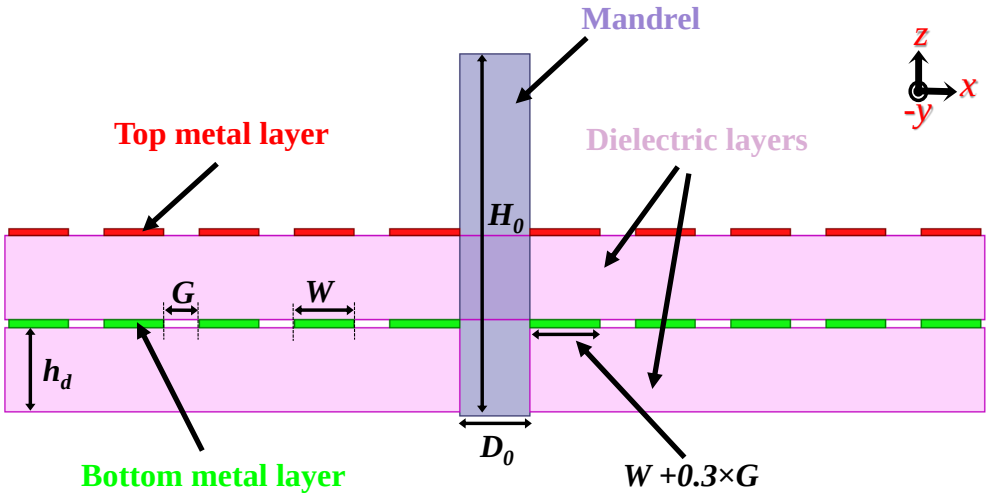

Figure 3.3. Cross-sectional view of the overlapped configuration at the rotation angle of θ=20°, which corresponds to the MDMD arrangement of layers.

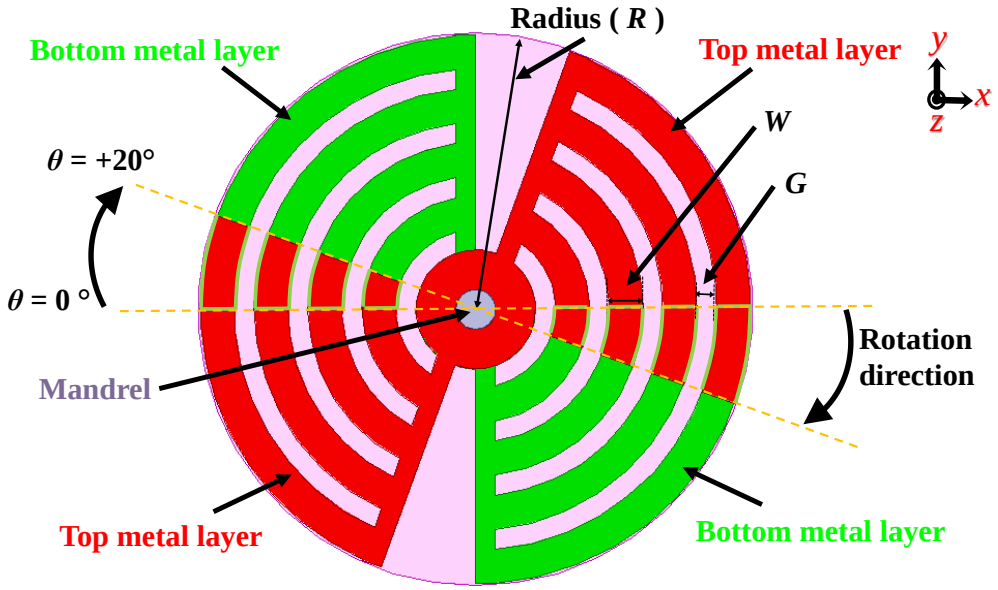

Figure 3.4. Top view of the overlapped configuration at the rotation angle of θ=20°, which corresponds to the MDMD arrangement of layers.

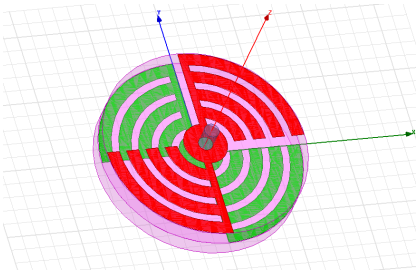

(a) θ= 0°

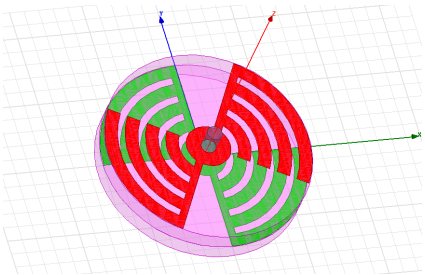

(b) θ= 30°

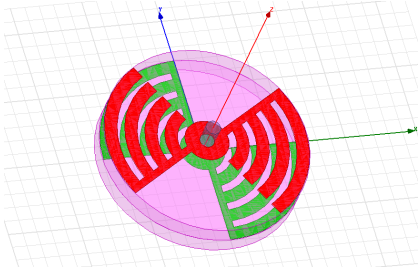

(c) θ= 60°

Figure 3.5. Different rotation positions (θ) of the MDMD configuration.

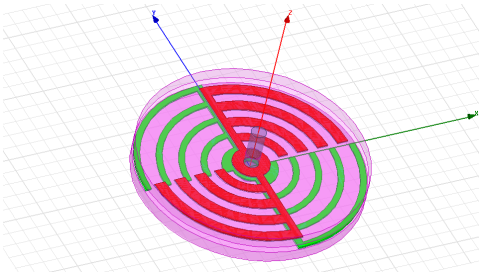

(a) θ= 0°

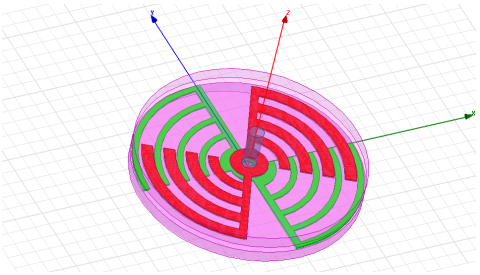

(b) θ= 30°

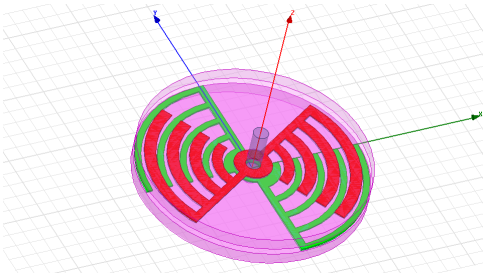

(c) θ= 60°

Figure 3.6. Different rotation positions (θ) of the DMMD configuration.

3.1.2 Antenna Part

The interrogating antenna used in the measurements, depicted in Fig. 3.7, is a single-slot microstrip antenna based on the design given in [39]. The antenna is redesigned to operate around 2 GHz. It has an approximate bandwidth of 10% for $\mid S_{11} \mid < 10$ dB. The slot part is on the front side of the substrate facing the rotation sensor, and is fed via a microstrip line at the back of the substrate. The feeding microstrip line is along the x-direction resulting an x-polarized electric field being transmitted from the slot, which corresponds to $\theta = 0°$ for the rotation sensor.

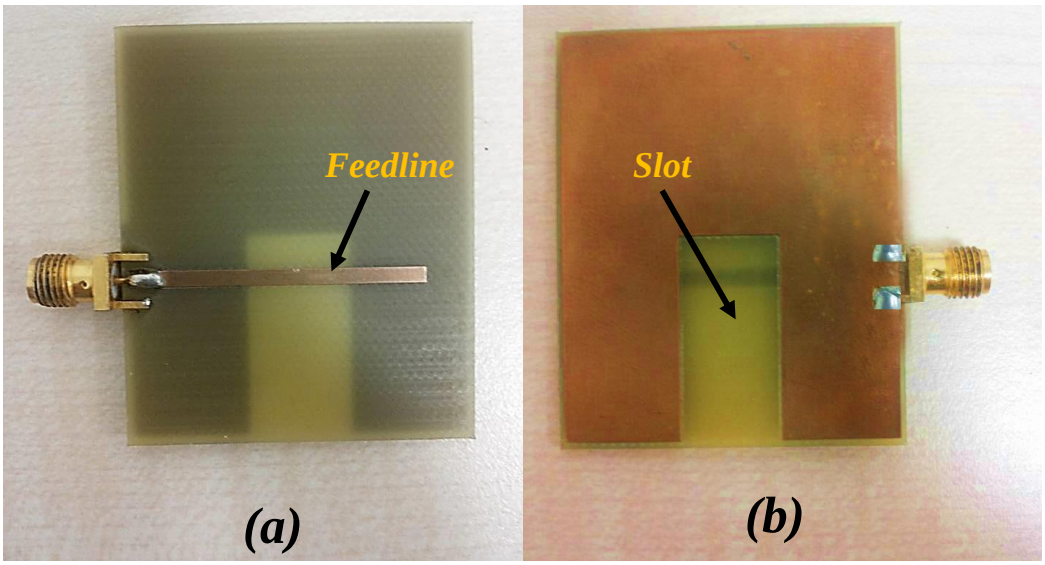

Figure 3.7. Fabricated microstrip single-slot antenna: a) Backside with the feedline and b) front side with the slot.

3.2 Modeling of the Sensing System

3.2.1 Parametric Tests for Local Optimization of the Proposed Sensor

Our sensor was designed and locally optimized based on scanning the parameters (W, G, and N) in specific intervals and incremental steps. In simulations, N was scanned from 2 to 6 with a step size of 1. G and W both were scanned from 0.5 to 3.1 mm with an incremental step of 0.3 mm. R is equal to $(5\times G+5\times W+8\times G_d+D_0/2)$ for DMMD configuration and $(4.3\times G+5\times W+9\times G_d+D_0/2)$ for MDMD configuration. The goal of the parametric variation was to find the best set of design parameters in a systematic way to achieve high sensitivity. There are $5\times 13\times 13$ possible sets of data for each configuration (totally 845 sets for each configuration), and for the sake of brevity, only a portion of the systematic variation is shown in Tables 3.1 to 3.3. In each table, one parameter is varied while the other two parameters are kept constant. In Table 3.1, N is scanned while W and G are kept at 1.7 and 1.1 mm, respectively. Then, in Table 3.2, W is tuned, whereas N and G are fixed to 4 fingers and 1.1 mm, respectively. Finally, the variation of G is tabulated in Table 3.3, while W and N are kept unchanged with the respective values of 1.7 mm and 4 fingers.

Table 3.1. Sensitivity (MHz/Degree), S levels compared for DMMD and MDMD configurations based on the simulation results ($W = 1.7$ mm, $G = 1.1$ mm).

N	**Rotation range (°)**	S_{DMMD}	S_{MDMD}
2	0 to 20	20	15
3	0 to 20	26	16
4	**0 to 20**	**28**	**18**
5	0 to 20	27	13
6	0 to 20	25	11

Table 3.2. Sensitivity (MHz/Degree), S levels compared for DMMD and MDMD configurations based on the simulation results ($G = 1.1$ mm, $N = 4$).

W	**Rotation range (°)**	S_{DMMD}	S_{MDMD}
0.5	0 to 20	24.2	15.87
0.8	0 to 20	25.45	16.94
1.1	0 to 20	26.7	17.42
1.4	0 to 20	27.6	17.61
1.7	**0 to 20**	**27.95**	**18.04**
2.0	0 to 20	27.65	18.12
2.3	0 to 20	27.64	18.22
2.6	0 to 20	27.61	18.17
2.9	0 to 20	27.61	18.23
3.1	0 to 20	27.42	18.15
3.4	0 to 20	27.13	18.13

Table 3.3. Sensitivity (MHz/Degree), S levels compared for DMMD and MDMD configurations based on the simulation results ($W = 1.7$ mm, $N = 4$).

G	**Rotation range (°)**	S_{DMMD}	S_{MDMD}
0.5	0 to 20	24.2	17.19
0.8	0 to 20	25.45	17.5
1.1	**0 to 20**	**27.95**	**18.04**
1.4	0 to 20	27.61	18.12
1.7	0 to 20	27.73	18.15
2.0	0 to 20	27.78	18.09
2.3	0 to 20	27.75	17.96
2.6	0 to 20	27.68	17.91
2.9	0 to 20	27.62	17.77
3.1	0 to 20	27.61	17.56
3.4	0 to 20	27.13	17.48

After comparing the simulation results of the two configurations, it is concluded

that DMMD configuration provides higher sensitivity. The finalized values of the locally optimized parameters are shown in Table. 3.4.

Table 3.4. Finalized design parameters for DMMD configuration.

N	G	W	R
4	1.1 mm	1.7 mm	16.3 mm

3.2.2 Numerical Simulation Setup

Each configuration was initially simulated inside a waveguide under appropriate excitation and boundary conditions. As illustrated in Fig. 3.8, the sensor was placed in the middle of a waveguide. The boundary conditions were chosen in a way that the lateral surfaces with the normal vector components ($\vec{n} = +\hat{y}$) and ($\vec{n} = -\hat{y}$) were taken as perfect magnetic conductors (PMCs), and the top ($\vec{n} = -\hat{x}$) and bottom ($\vec{n} = +\hat{x}$) surfaces as perfect electric conductors (PECs). This selection of the boundary conditions yields plane wave propagation in which electrical and magnetic fields are simultaneously perpendicular to each other and to the direction of propagation (in $\hat{z}$ direction). The designed sensor was placed to face the ports and the traveling E-fields were parallel to the θ= 0° position of the sensor. In order to obtain linearly polarized E-and H-fields over the sensor, surface of each port was considered five times greater than the surface of the sensor.

Since our sensing system consists of two main elements, which are the rotation sensor and the interrogating antenna, it is required to verify results of the waveguide simulation with another systematic simulation. Therefore, the finalized metamaterial-inspired rotation sensor was again simulated beside an antenna (see Fig. 3.9). In this systematic simulation instead of deploying a waveguide, the proposed microstrip slot antenna (which is discussed in Section 3.1.2) was placed in front of the sensor within a fixed distance. Again, the polarization of E-field that excites the sensor was parallel to the $\theta = 0°$ position of the rotation sensor.

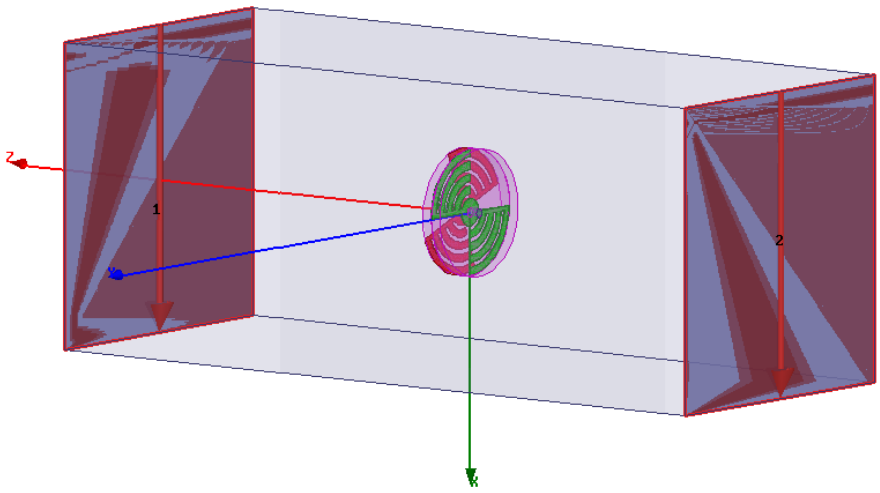

Figure 3.8. Simulating the proposed sensor inside a waveguide.

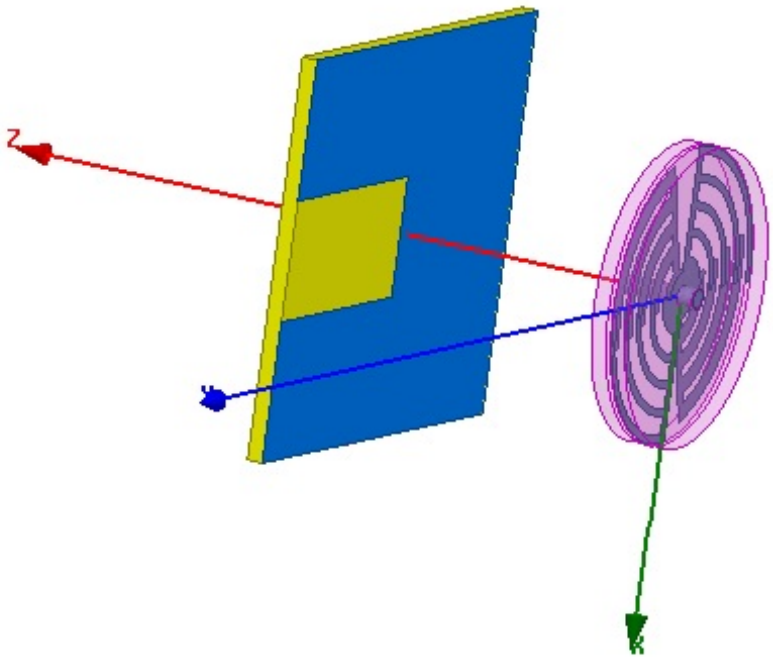

Figure 3.9. Simulating the proposed sensor beside the antenna.

Fig. 3.10 presents the frequency shift versus rotation angle of the finalized design for both of the simulation setups. As it is expected, simulating our sensor inside the waveguide or beside the antenna yields similar results.

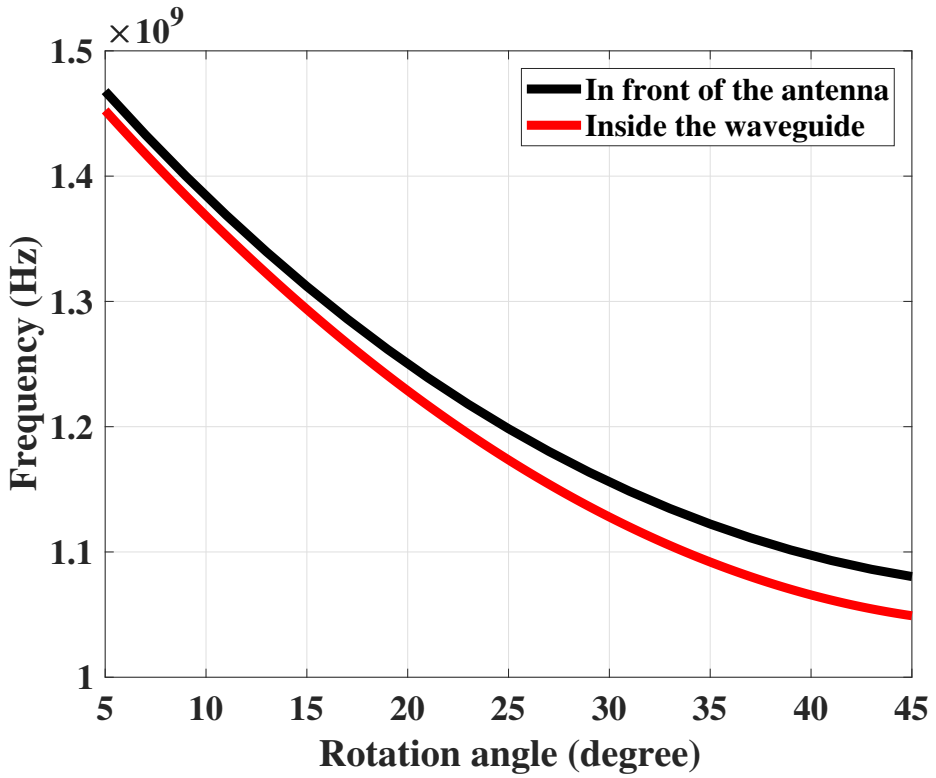

Figure 3.10. Comparing the results obtained from the simulation of the sensor beside the antenna and inside the waveguide by investigating the frequency shift versus rotation angle for each simulation setup.

Finally, the desired sensor was fabricated, which is shown in Fig. 3.11, and its performance was characterized by experimental measurements and compared with systematic simulation results in Section. 4.1.

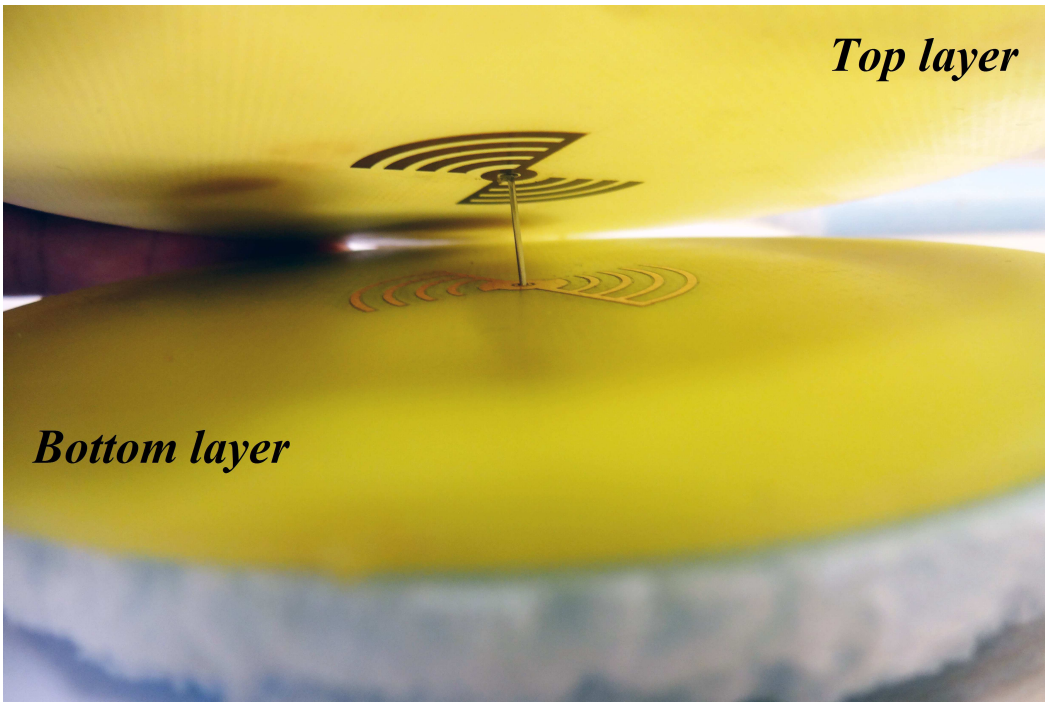

Figure 3.11. Top and bottom layers of the fabricated sensor.

Chapter 4

Experimental Results and Discussions

This chapter is based on the prepared journal article "A Wireless Metamaterial-Inspired Passive Rotation Sensor with An Unprecedented Submilliradian Level of Resolution" by A. Maleki Gargari, B. Ozbey, H. V. Demir, A. Altintas, U. Albostan, O. Kurc, V. B. Erturk, *in submission*, 2017, which is reproduced (or 'reproduced in part') with permission [40].

For understanding the characteristics of our sensor design in operation for real-life applications, four sets of experiments were performed on the rotation sensor. The bottom layer of the sensor was fixed over a standard protractor, while the top layer was rotated to assess its performance metrics including sensitivity, linearity, dynamic range, and resolution. The center part of the protractor, over which the sensor was placed, is removable. Therefore, experiments were initially performed without it, where the sensor was mounted on a dielectric Styrofoam. Then, experiments were repeated when the sensor was mounted on a metallic sheet so that its effects on the aforementioned figures-of-merit could be investigated. The arrangements of the sensor over the both background objects and protractor are presented in Fig. 4.1.

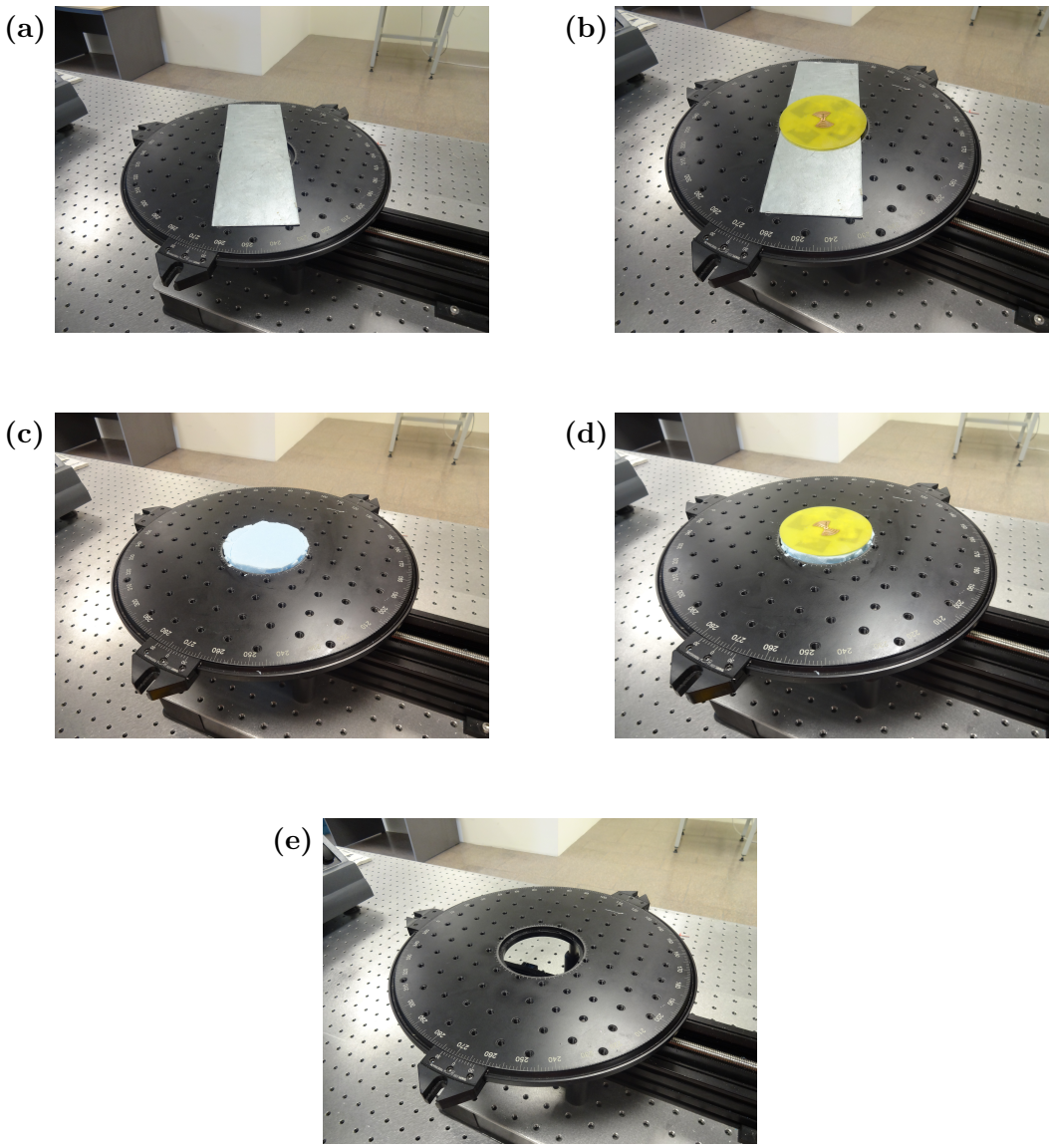

Figure 4.1. The arrangement of the sensor and background objects (a)-(e): (a) The metallic sheet positioned over the protractor. (b) The bottom layer of the sensor positioned over the metallic sheet and the protractor. (c) The dielectric Styrofoam positioned in the middle of the protractor. (d) The bottom layer of the sensor positioned over the dielectric Styrofoam and the protractor. (e) The standard circular protractor.

In the first set of experiments, two parts of the sensor were moved interdigitally inside each other with a coarse level of rotation (i.e., 5° or 10°). As it is presented in Fig. 4.2, a fork-like three-stick configuration with a length of $L_s = 50$ cm (all sticks with a diameter of 1 cm) was applied to ensure more stable rotation by increasing the bending stiffness of the sticks during the measurements. The fork part was fixed on the top dielectric layer of the sensor and its handle part was used to rotate the sensor over the protractor. Besides, the radius of FR-4 substrates in top and bottom layers was increased to 4 cm and WD-40 brand grease was applied to the air gap, G_a, between the top and bottom metallic layers to minimize friction and vibration related mechanical problems. By rotating the top layer over the fixed bottom layer, the resonance frequency of the coupled system of antenna and sensor was varied, which was recorded using a vector network analyzer (VNA) for different rotation angles. Eventually, the sensitivity was obtained by extracting the slope of the measured resonance frequency-rotation angle curve.

In the second set of experiments, the maximum rotation range where the linearity error was taken below 5% (defined as the dynamic range) was investigated, and in the third set of experiments, the variation of the rotation range with respect to the separation between the antenna and the top layer of the sensor (defined as the monitoring distance, D_m) was explored. In the fourth set of experiments, various tests were carried out to obtain submilliradian level of resolution. The fork part of the wooden stick was fixed on the top dielectric layer of the sensor while its handle part was connected to the moving part of a translation stage with flexible adhesive blu-tack, by means of which a precisely controlled linear movement was converted to a micron-level controlled-rotation on the sensor.

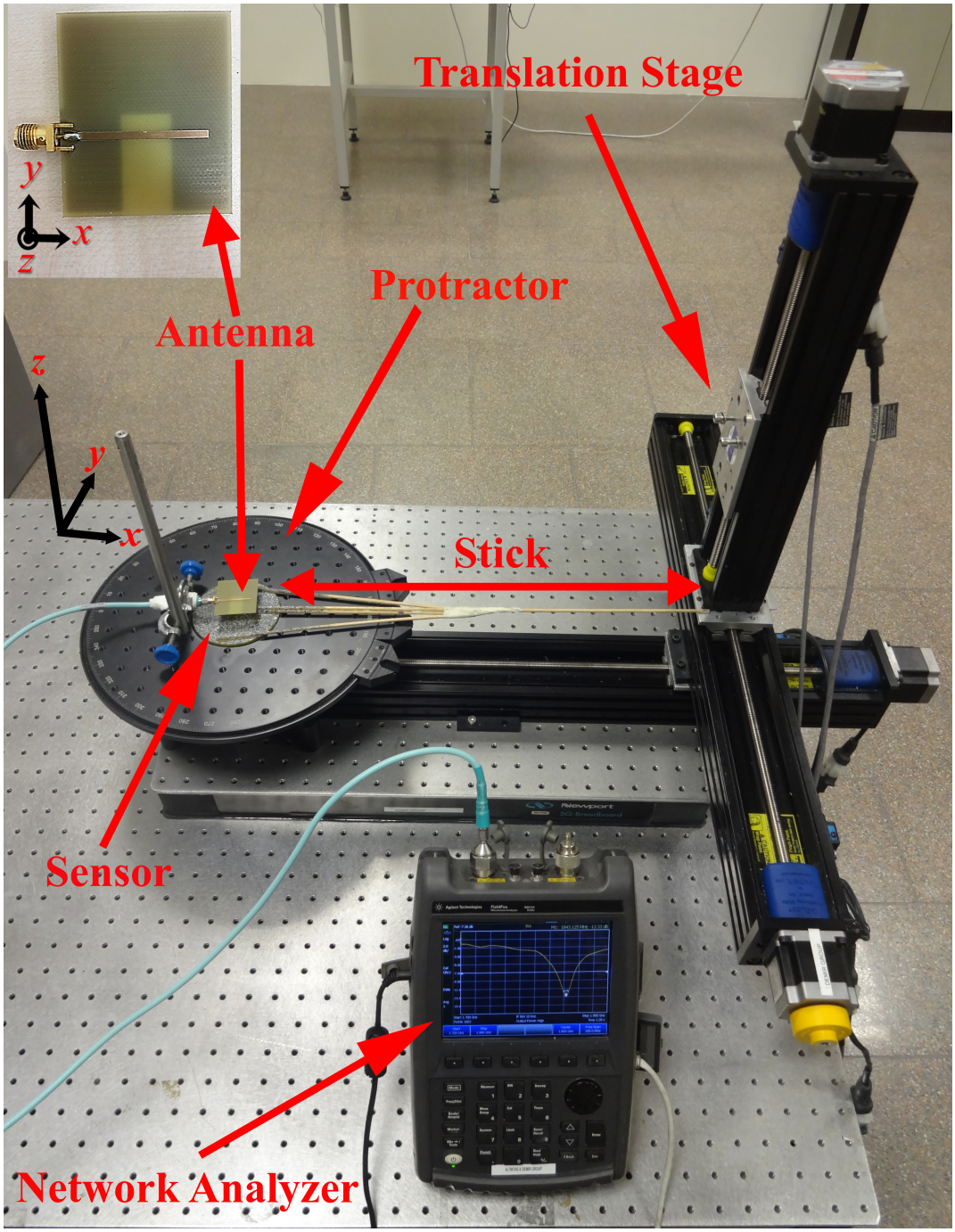

Figure 4.2. Experimental setup prepared for the resolution test.

4.1 Sensitivity

The first step in characterizing our sensor was to measure its sensitivity. As depicted in Figs. 4.3 and 4.4, the resonance of the coupled system manifests itself in the form of a dip when $\mid S_{11} \mid$ is monitored via a VNA. Here, the sensor was positioned on a dielectric layer and a metallic sheet, respectively, where the shifts in the resonance frequency can be clearly seen as the sensor rotates from 5° to 45° with 5° steps. As expected, by increasing the rotation angle (θ), the interdigital area was expanded, and the equivalent capacitance of the system was accordingly increased which yields in a decrease in the resonance frequency.

Fig. 4.5 presents the shift in frequency versus the rotation angle for both experimental and simulation results, when the sensor was on a Styrofoam dielectric layer and a metallic sheet. The experimental data were the average of ten different measurements for each case, and the simulations were carried out in Ansoft HFSS. A reasonable agreement between the measurements and the simulations are observed. Exclusion of grease in the simulations, manufacturing tolerances and uncertainties in some dimensions (in particular, the air-gaps, G_a and G_d) are considered as the potential sources of discrepancies especially in small θ values.

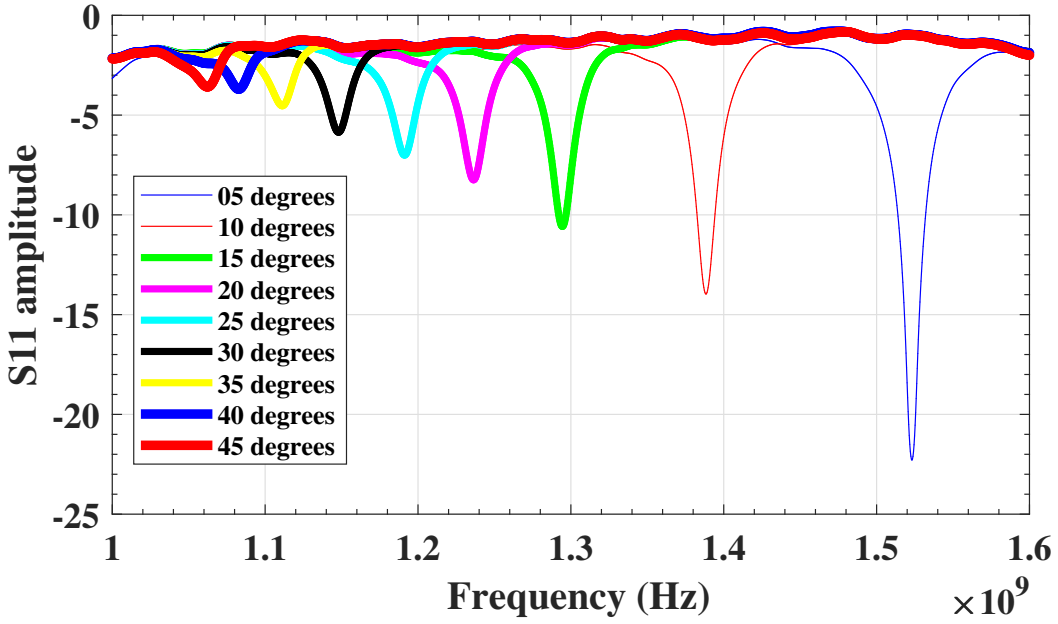

Figure 4.3. Shifting S_{11} magnitude curves over dielectric Styrofoam.

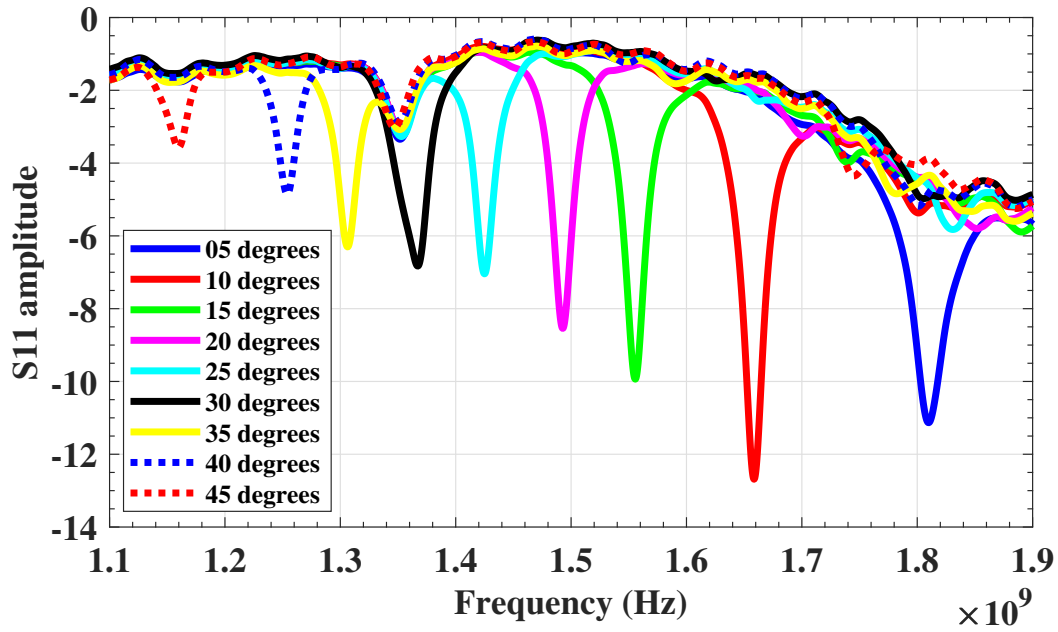

Figure 4.4. Shifting S_{11} magnitude curves over metallic sheet.

Sensitivity, which describes the amount of spectral change read out telemetrically from the sensor in response to the rotation, can be mathematically defined as the slope of the frequency-rotation angle curve, presented in Fig. 4.5, with a unit of MHz/degree. For various 5° rotation ranges, the extracted sensitivity levels of the sensor for both dielectric layer and metallic sheet cases are respectively tabulated in Tables 4.1 and 4.2. As can be seen from the tables (as well as from Fig. 4.5), sensitivity of the sensor was very high at low rotation angles for both cases (26.4 MHz/degree for the dielectric case and 28.8 MHz/degree for the metallic sheet case when $5° \leq \theta \leq 10°$ interval) but decreases at higher rotation angles.

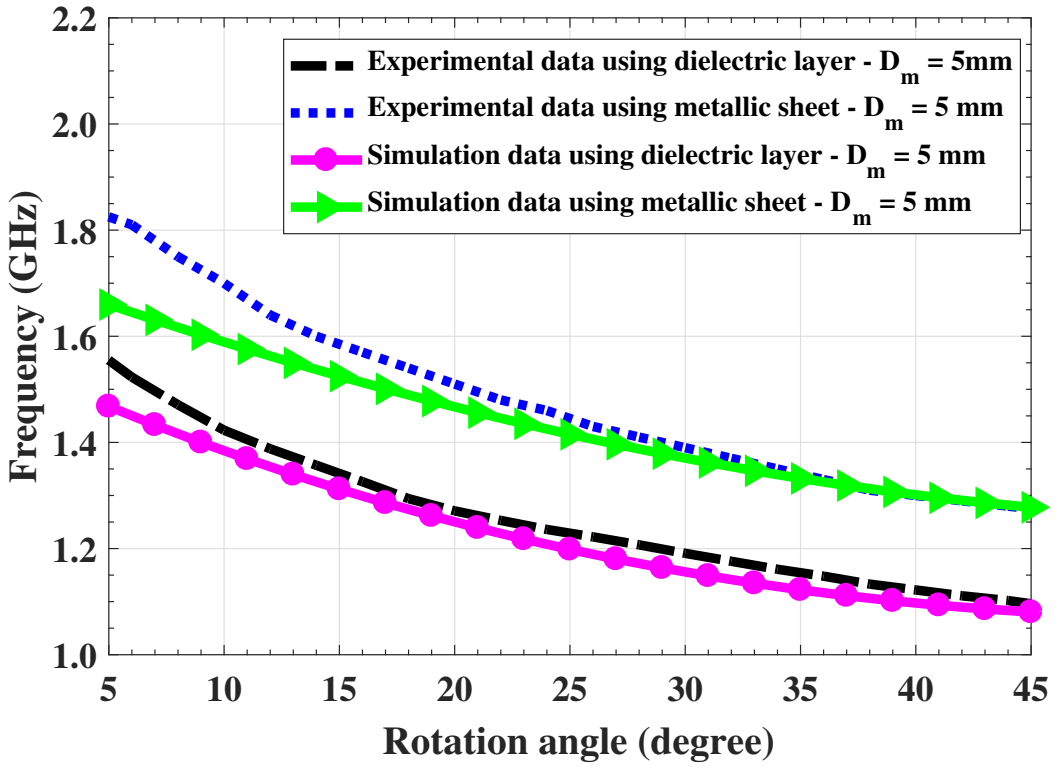

Figure 4.5. Shift in the operating frequency versus the rotation angle.

As listed in Tables 4.1 and 4.2, R^2 parameter [41] was used to assess the linearity of the sensor. The R^2 value is over 0.99 in every 5° rotation range for both dielectric layer and metallic sheet cases. This feature indicates not only a high linearity but also exhibits another advantage of the sensor that it can be

utilized in several initial rotation angles without sacrificing its linear response. Simply, allowing an initial θ on the sensor to create a frequency offset, the sensor can be employed in higher rotation angle operation regions depending on the linearity and the resolution of that region of choice.

Table 4.1. Experimental results of the sensitivity test and R^2 parameter for several selected rotation ranges using the dielectric layer.

Over Styrofoam layer		
Rotation range (°)	**Sensitivity (MHz/degree)**	**R-squared**
5 to 10	26.40	0.99
10 to 15	19.28	0.99
15 to 20	14.83	0.99
20 to 25	9.64	0.99
25 to 30	7.36	0.99
30 to 35	7.30	0.99
35 to 40	6.52	0.99
40 to 45	5.07	0.99

Table 4.2. Experimental results of the sensitivity test and R^2 parameter for several selected rotation ranges using the metallic sheet.

Over metallic sheet		
Rotation range (°)	**Sensitivity (MHz/degree)**	**R-squared**
5 to 10	28.80	0.99
10 to 15	23.20	0.99
15 to 20	17.07	0.99
20 to 25	14.15	0.99
25 to 30	13.91	0.99
30 to 35	12.05	0.99
35 to 40	8.27	0.99
40 to 45	6.30	0.99

4.2 Dynamic Range

The linearity degrades as the rotation range is increased. Thereby, instead of investigating piecewise linearity, one can check the maximum linear range of the proposed sensing system. Dynamic range is defined here as the maximum rotation range that can be read out under the constraint that $R^2 > 0.95$. Table 4.3 lists the R^2 parameter for different rotation ranges. Based on the given definition, the dynamic range of this sensor was found approximately 40°.

Table 4.3. Identification of the maximum dynamic range based on R^2 parameter.

R-squared		
Rotation range (°)	**Metallic sheet**	**Styrofoam dielectric**
5 to 10	0.997	0.998
5 to 15	0.987	0.985
5 to 20	0.978	0.984
5 to 45	0.954	0.964
5 to 50	0.935	0.946

4.3 Rotation Tracking Range and Monitoring Distance

The rotation tracking range, defined as the maximum rotation range that can be captured by the antenna, can easily reach 75° by decreasing the monitoring distance, D_m, which is the distance between the antenna and the sensor. This feature was investigated in a fashion similar to that described in [42] for both background objects. Fig. 4.6 shows the rotation tracking range of the rotation sensor for various monitoring distances (D_m). It should be noticed that the one-to-one relationship between the rotation angle and the corresponding resonance frequency is independent of the antenna's position with respect to the sensor; that is, the measured shift in the resonance frequency of the coupled system

(appearing in the form of a dip in | S_{11} | spectrum) corresponds to the same rotation angle. Considering a tracking threshold of 1 dB [42], the entire rotation range of 75° can be tracked by the antenna if D_m is decreased to 5 mm.

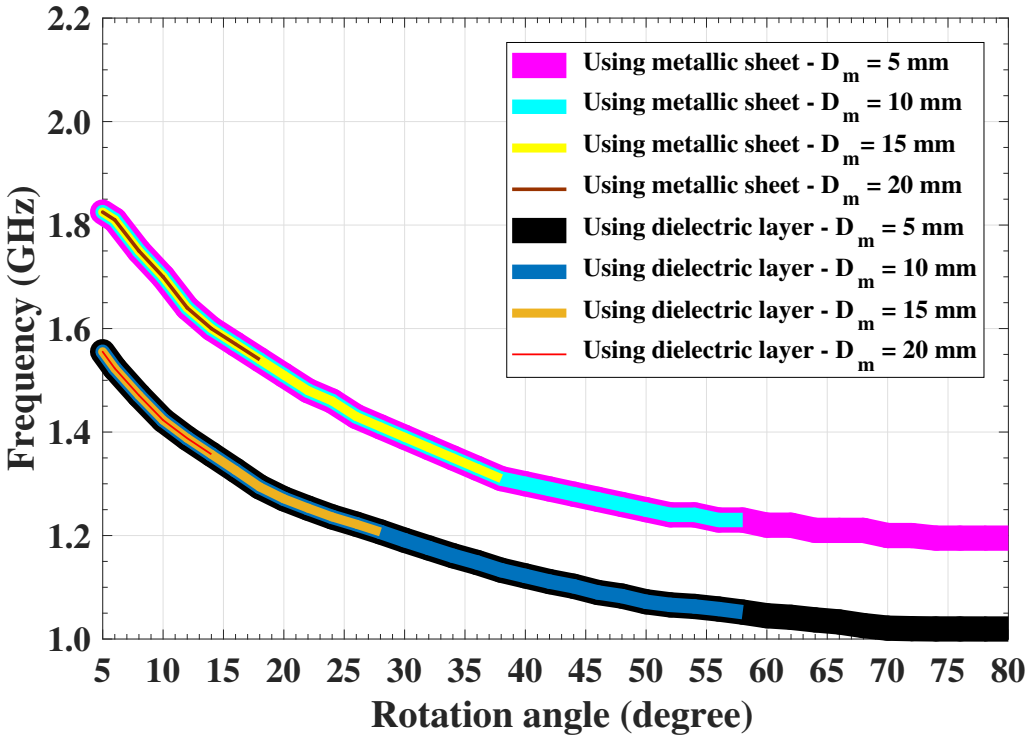

Figure 4.6. Rotation tracking range versus the monitoring distance for both dielectric and metallic sheet backgrounds.

However, increasing the monitoring distance reduces the dynamic range, and based on the experimental results, rotation tracking range in the dielectric case decreases quicker than the metallic sheet case. For instance, when D_m increases to 20 mm, the rotation tracking range reduces nearly to 9° for the dielectric case and 13° for the metallic case. Therefore, to determine the maximum monitoring distance, only the worst case scenario was considered. Fig. 4.7 shows the rotation tracking range of the sensor over the dielectric layer for longer monitoring distances. As observed in Fig. 4.7, the dynamic range for the dielectric layer falls down to 6° for a monitoring distance of 60 mm (when using a tracking threshold of 1 dB). One can reduce the tracking threshold value to further improve the

monitoring distance, however this improvement is limited by the system noise.

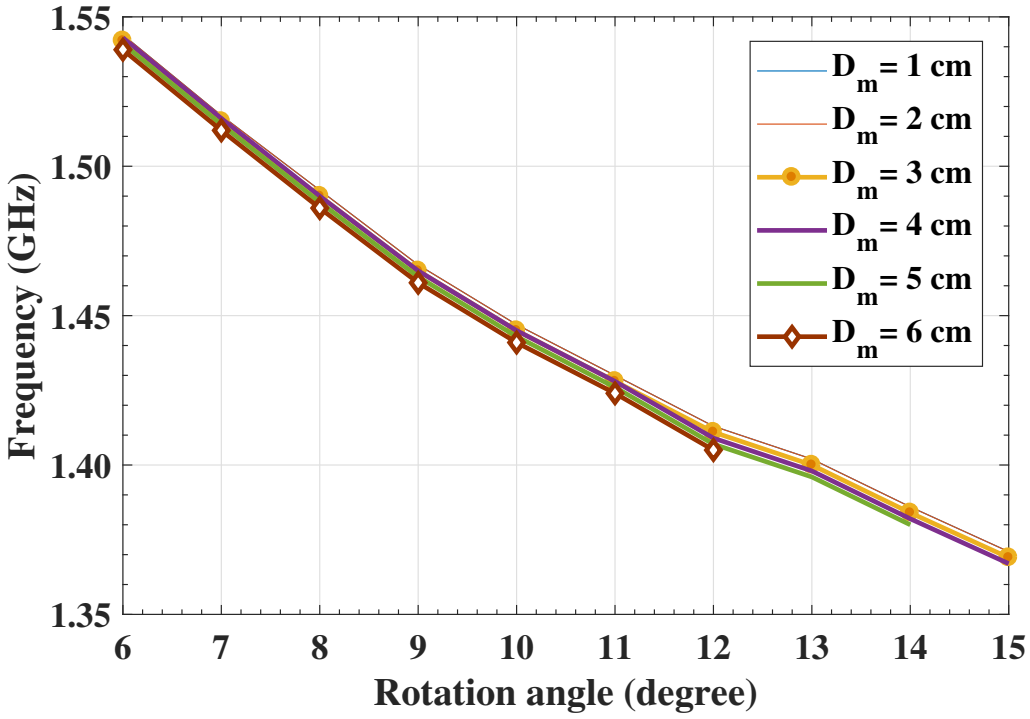

Figure 4.7. Rotation tracking range when using dielectric Styrofoam for higher monitoring distances.

4.4 Resolution

4.4.1 Resolution Test of Sensing System

In real-life applications, rotation-based bendings happen in very small angles. In this section, the capability of the sensor in measuring submilliradian rotation levels was investigated.

In our experimental setup, the minimum rotational displacement that could be created by the translation stage was 10 μ-radians. In order to determine the resolution of the sensing system, extensive experiments were performed on the sensor for different values of rotational displacements. More precisely, the experiments were conducted for rotational displacements with step sizes of 200, 150, 100, 80, 40, 20, and 10 μ-radians. The sensor could resolve the rotational displacement in all of these experiments except in the case with the step size of 10 μ-radians. Hence, it is safe to conclude that the resolution level of the proposed sensing system is 20 μ-radians.

Figs. 4.8 and 4.9 show the results of the resolution tests when using dielectric platform and metallic sheet, respectively, for a range of 12000 μ-radians. During the experiments, the first 200 steps were applied with a 40 μ-radian step size (corresponding to a total of 8000 μ-radians) and the next 200 steps were applied with a 20 μ-radian step size (corresponding to a total of 4000 μ-radians). The data used to generate both figures (Figs. 4.8 and 4.9) were taken with the IF bandwidth set to 1 kHz together with the averaging option of the VNA without any smoothing so that the system noise was included in the recorded data. After the data acquisition the raw data was filtered (with a low-pass filter) to remove the high-frequency fluctuations. Both filtered and unfiltered data are depicted in Figs. 4.8 and 4.9, presenting the resonance frequency read out from the sensor as a function of the rotation angle.

After every 100 steps, the experiments were paused for about 5 minutes. First of all, it can be seen in both Figs. 4.8 and 4.9, there is almost a flat portion with no

frequency change immediately after the pause, and then especially in the metallic sheet case there is a sudden frequency jump and afterwards the frequency changes almost linearly with the continuing rotation (the growing number of steps). The flat portions in both figures indicate that the motion of the translation stage is not fully transferred to the sensor through the wooden sticks most probably due to the initial stored mechanical energy in the flexible adhesive or the energy required to overcome the static friction (even though lubrication was applied) between the sensor layers. As larger displacement was applied through the transition stage to the system (number of steps was increased), a jump was observed, which indicates a sudden transfer of the total displacement to the sensor. Afterwards, the expected linear behavior was observed. Considering the first 200 steps and the next 200 steps, the slopes of the two linear regions in each group of 200 steps are relatively the same. The slope of every linear region (given in KHz/μrad) is displayed accordingly in both Figs. 4.8 and 4.9.

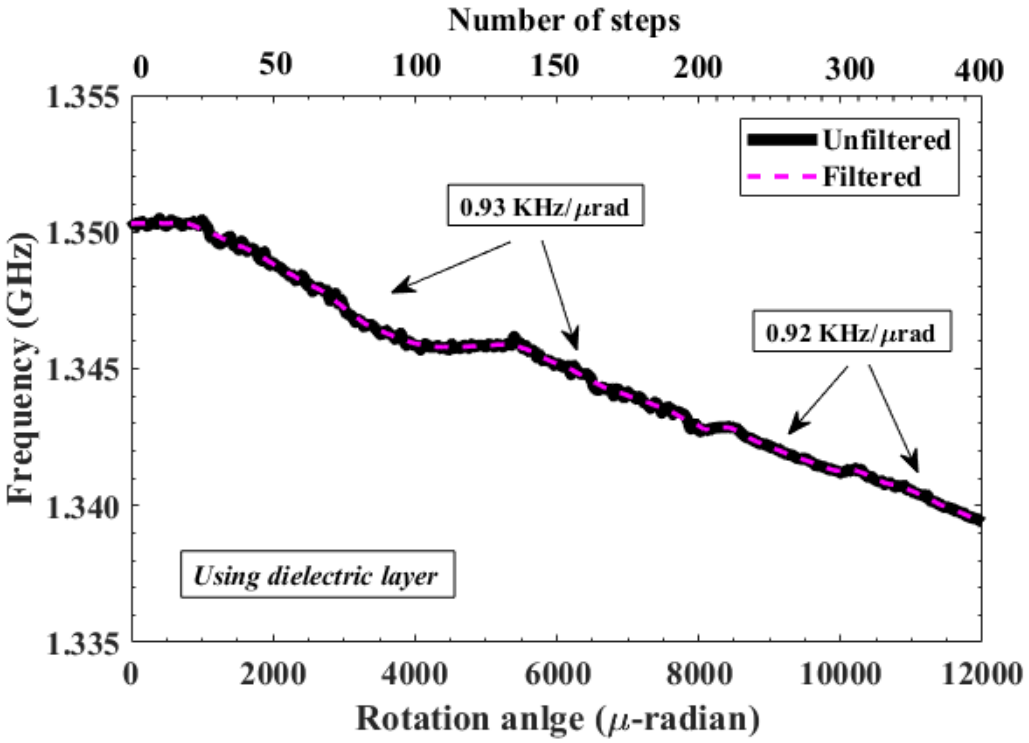

Figure 4.8. Resolution test using dielectric Styrofoam (with 5 min pausing after every 100 steps).

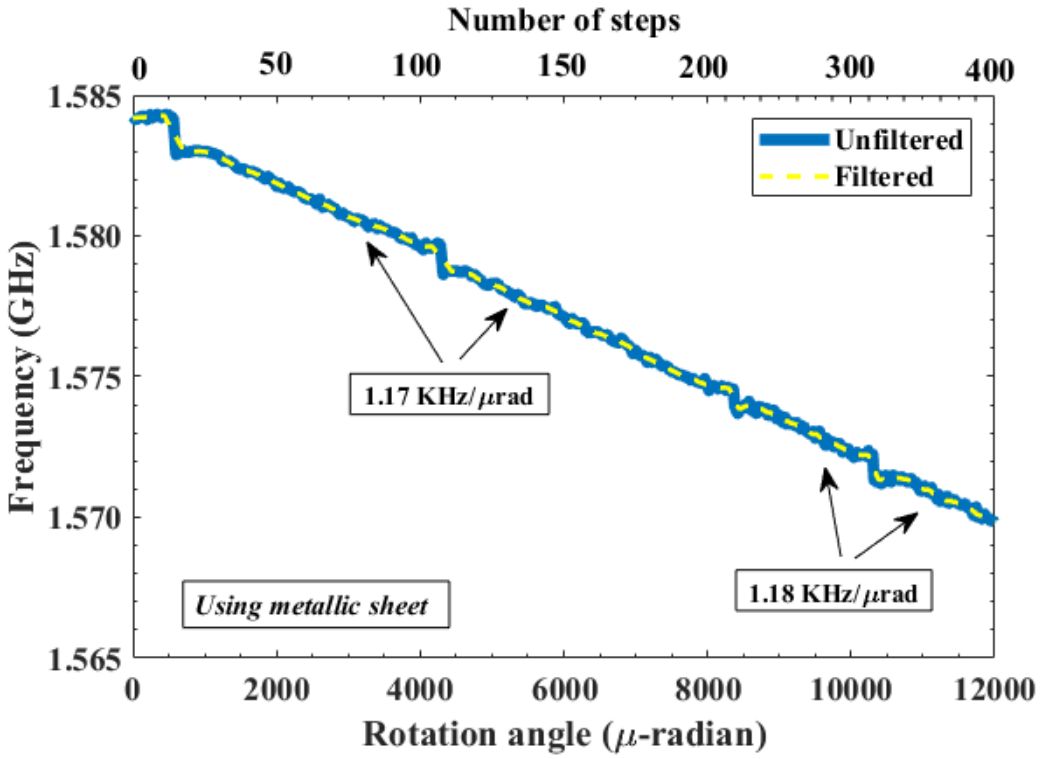

Figure 4.9. Resolution test using metallic sheet (with 5 min pausing after every 100 steps).

4.4.2 Resolution Verification Using Digital Image Correlation (DIC) Method

To study the resolution of the proposed sensor, digital image correlation (DIC) method was utilized. DIC provides information on displacement and deformation distribution across the whole imaged surface without any contact to the specimen [43]. The DIC method is based on tracking the movement of the selected points on speckle pattern by comparing at least two consecutive digital images. Subsequently, from the movement of the tracked points on the surface, the displacement and deformation distributions are calculated.

The setup of this experiment was configured as follows. First, the top surface of the sensor was speckled with black and white spray paints in such a way that the speckles were distributed randomly and homogeneously across the whole surface area (see Fig.4.10). Second, a digital camera was located such that its sensor plane was positioned parallel to the specimen surface. The camera was controlled by a computer to fully automize the image acquisition process. Finally, the setup was illuminated by a LED projector, which minimizes the noise on the camera sensor. In Fig. 4.11, the experimental setup is presented.

In this study, a Nikon D5200 DSLR camera was used for the image acquisition process. This camera had 24MP (6000×4000 pixels) and 2MP (1920×1080 pixels) resolutions for photo and video modes, respectively. Due to the quick loading and focusing on a very small surface area (1 pixel representing approximately 80 μm), the video mode was chosen for the image acquisition process. The camera was capable of shooting maximum 59.94 frames per second in the video mode and a total of 51,547 frames were taken for this experiment. Then, the images were extracted from video such that 30 frames were obtained for each one second interval. These 30 frames in each one second interval were averaged geometrically in order to minimize the noise on the images. Finally, 9,600 averaged images were created. The averaged images were correlated by using GOM Correlate software, which is free for the 2D measurement applications. After correlation, the resultant displacements of the points located at the outer edge of the surface were obtained

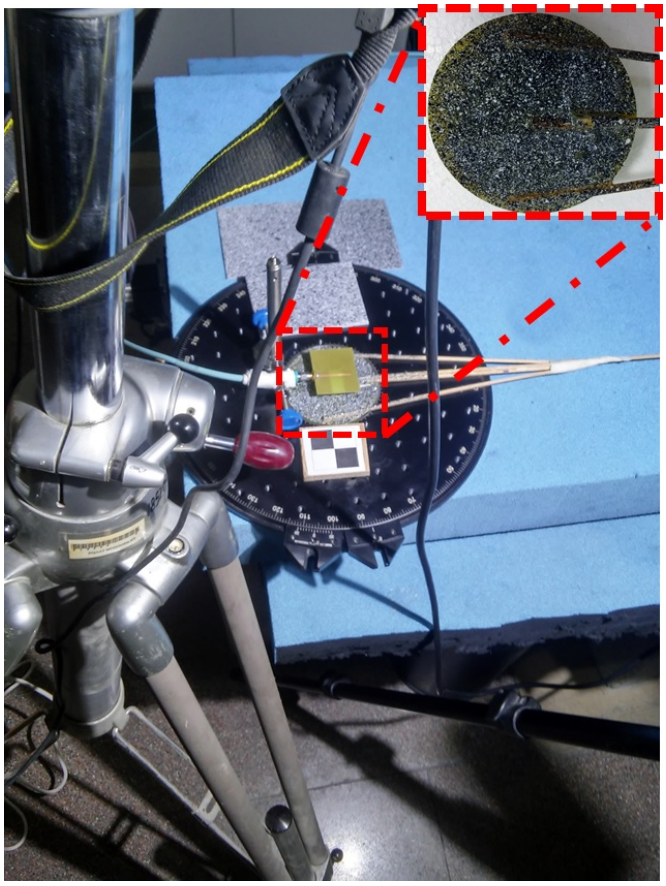

Figure 4.10. The black and white speckles over the sensor.

from the software and converted to the rotation angle.

The rotations measured by the DIC method, as explained above, are compared with the results obtained using the proposed rotation sensor. In Fig. 4.12, the results of the resolution characterization using a step size of 80 μ-radians, performed over dielectric layer background, are presented. Along with experimental data, a straight dashed-line was added to show the expected rotation created by moving the translation stage. There is a good agreement between the measurements using the DIC method and our sensor. As expected, the motion of the translation stage was not mechanically transferred fully to the top layer of the sensor, as the flat portion was completely observable for both measurements at the beginning of the movement, and the desired linear region occurred only after 4 steps (48 seconds).

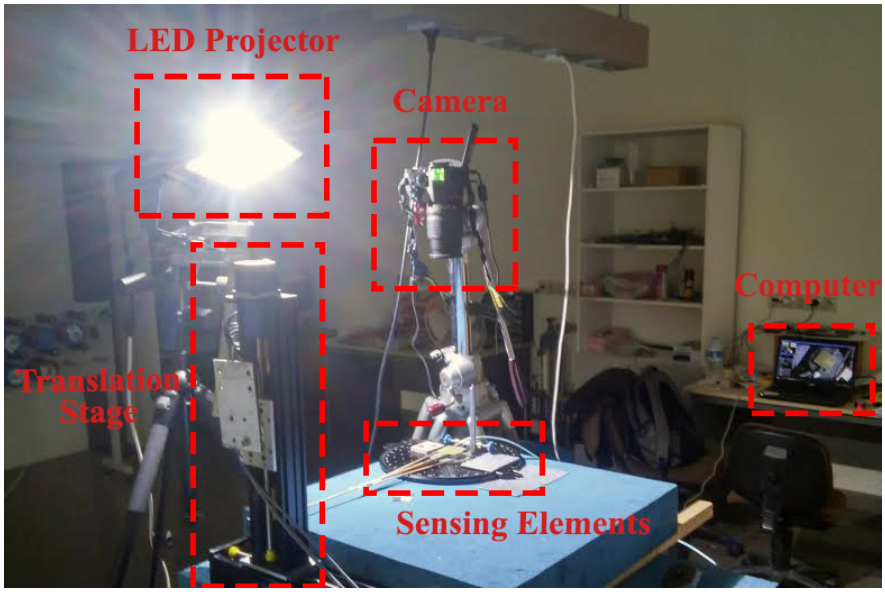

Figure 4.11. Experimental sensing setup, where DIC apparatus was also added.

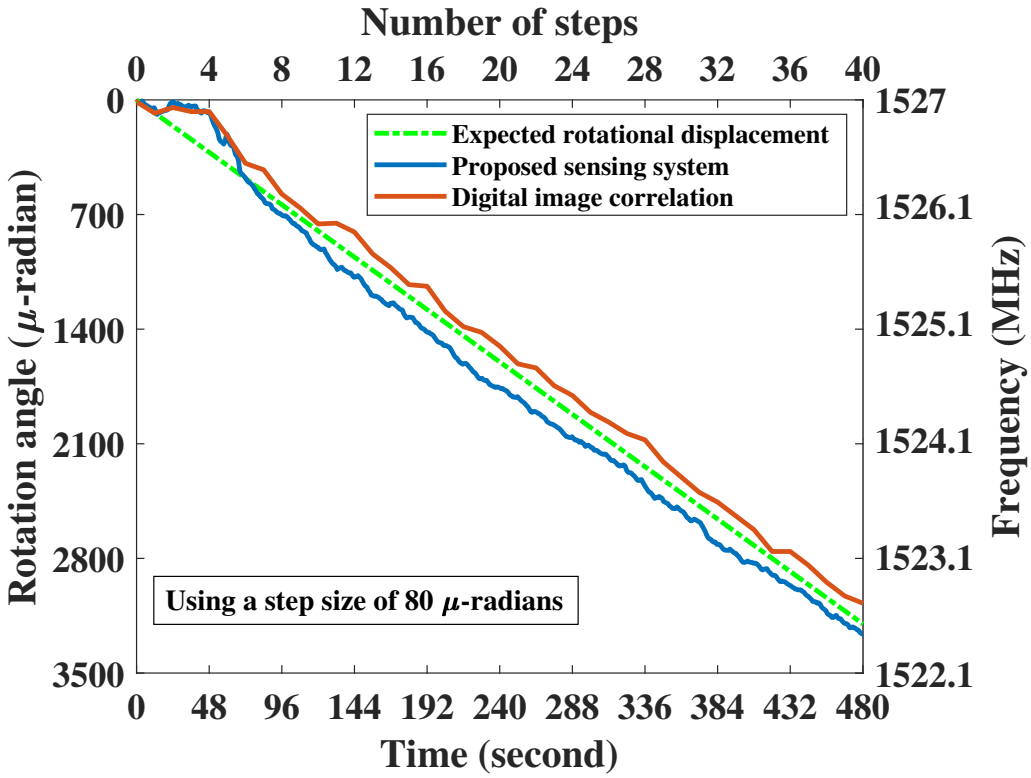

Figure 4.12. Comparing the experimental results of the proposed sensing method with the DIC method for a 80-μradian resolution level, shown along with the expected rotational displacement generated by moving the translation stage.

Chapter 5

Conclusion and Future Work

In conclusion, here a wireless metamaterial-inspired passive rotation sensing system was proposed and demonstrated for measuring the bendings in μ-radian regime. Since the primary goal of this system was to measure telemetrically very tiny amounts of bending in the elastic deformation region, the performance metrics of resolution and sensitivity were more important than other figures-of-merit of the sensor. Previously, as there was no wireless technology that had been developed to measure such μ-radian range bendings, this thesis is the first account of μ-radian wireless rotation sensing, to the best of our knowledge.

In this thesis, for specific SRR architectures, interdigital and overlapping configurations were introduced while designing the proposed rotation sensor. Each configuration was initially simulated inside a waveguide, and then the design parameters were locally optimized to achieve the highest sensitivity in each case. The interdigital configuration was found to display higher sensitivity compared to the overlapping configuration. Thus, it was chosen as the finalized design for fabrication purposes. Additionally, a single-slot microstrip antenna was redesigned and fabricated to read out and monitor telemetrically the rotation of the proposed sensor by following the variations in frequency response of the coupled antenna-sensor system. To mimic possible applications of the proposed sensor in real-life scenarios, all of the characterization experiments were performed over

two different background objects, namely, metallic sheet and Styrofoam dielectric platform.

Based on our proof-of-concept demonstration, the proposed wireless rotation sensing system exhibited excellent resolution (<20 μ-radians) and high sensitivity (>28 MHz/degree). In addition, linearity of the sensor was investigated using coefficient of determination (R^2 parameter). The experimental results showed that the rotation angle-frequency response of the proposed system is 95% linear over a span of 40°. Furthermore, the rotation tracking range of the sensor can be extended to 75° by decreasing the monitoring distance to 5 mm. Finally, the resolution of the sensor was determined by rotating it in very fine discrete steps and processing the shifts telemetrically read out from the dips of the resonance frequency. The designed sensor was shown to successfully resolve the rotational displacements as low as 20 μ-radians. Also, the resolution performance of the sensor was validated by using DIC method at the limit of the camera system (which was 80 μ-radians in our setup). These findings indicate that the developed rotation sensor holds great promise for industrial applications.

A future study in the direction of this thesis may include designing an array of sensors for measuring rotation-based bendings in an elongated load carrying elements (e.g., steel beams). As it is illustrated in Fig. 5.1, the bottom layer of the each sensor can be fixed on the neutral-axis on the body of a beam, while the top layer is fixed to two points with equal vertical distance from the neutral-axis by using a specific stick with sufficient length and rigidity. In this way, the contraction in the upper part and the elongation in the bottom part of the neutral axis can be transformed by the sticks to the rotation with the centrality in the sensor. Therefore, by forming a linear array of these sensors along the length of the beam, elastic deformations associated with the beam can be obtained at many points. Finally, by using the rotation readings from each of the sensor and applying the beam elastic theory, various required parameters such as displacement, beam inner forces, and load applied to the beam can be calculated for any beam given its boundary conditions.

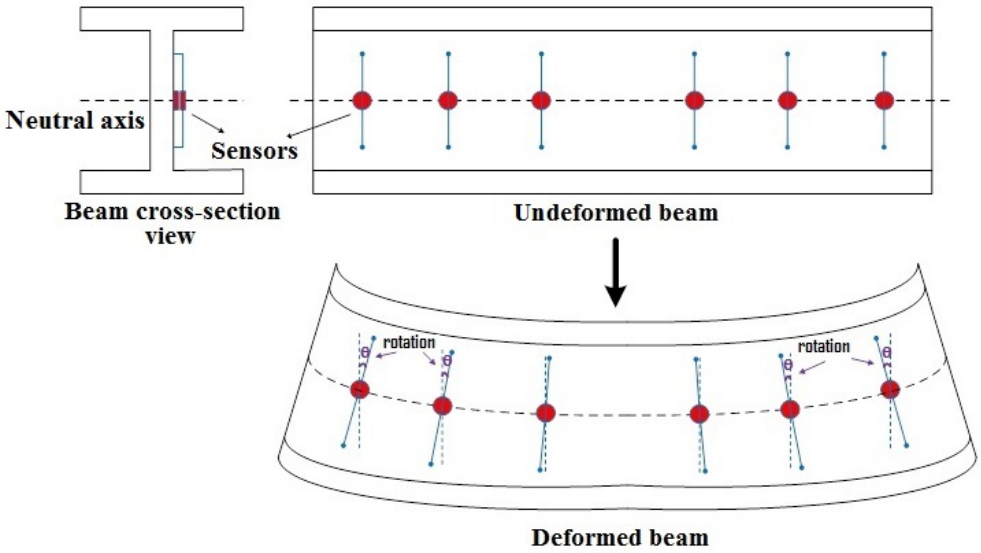

Figure 5.1. Assembling procedure of multiple sensors along a beam.

Another discussion that can be considered as the future step may target at increasing the monitoring distance. The maximum D_m that was achieved using the proof-of-concept demonstrator sensor was 6 cm, which may deem relatively short for some of the real-life applications. A possible approach to increase D_m can rely on deploying semi-passive devices. Such devices are commonly used in RFID and energy harvesting applications, and can be switched on and off by converting a small RF signal into a DC bias current. This RF signal is amplified inside the device and finally an internal transmitter reflects it back to the desired direction. Such amplified signal may aid us to track the rotation in farther distances.

The results of this thesis work, are also included in the prepared journal article "A Wireless Metamaterial-Inspired Passive Rotation Sensor with An Unprecedented Submilliradian Level of Resolution", which is in submission [40].

Bibliography

[1] J. B. Pendry, A. J. Holden, D. J. Robbins, and W. J. Stewart, "Magnetism from conductors and enhanced nonlinear phenomena," *IEEE Transactions on Microwave Theory and Techniques*, vol. 47, no. 11, p. 2075, 1999.

[2] D. R. Smith, W. J. Padilla, D. Vier, S. C. Nemat-Nasser, and S. Schultz, "Composite medium with simultaneously negative permeability and permittivity," *Physical review letters*, vol. 84, no. 18, p. 4184, 2000.

[3] R. Shelby, D. Smith, S. Nemat-Nasser, and S. Schultz, "Microwave transmission through a two-dimensional, isotropic, left-handed metamaterial," *Applied Physics Letters*, vol. 78, no. 4, p. 489, 2001.

[4] R. Marqués, F. Mesa, J. Martel, and F. Medina, "Comparative analysis of edge-and broadside-coupled split ring resonators for metamaterial design-theory and experiments," *IEEE Transactions on Antennas and Propagation*, vol. 51, no. 10, p. 2572, 2003.

[5] F. Falcone, T. Lopetegi, J. D. Baena, R. Marqués, F. Martín, and M. Sorolla, "Effective negative-/spl epsiv/stopband microstrip lines based on complementary split ring resonators," *IEEE Microwave and Wireless Components Letters*, vol. 14, no. 6, p. 280, 2004.

[6] S. N. Burokur, M. Latrach, and S. Toutain, "Study of the effect of dielectric split-ring resonators on microstrip-line transmission," *Microwave and Optical technology letters*, vol. 44, no. 5, p. 445, 2005.

[7] T. Koschny, M. Kafesaki, E. Economou, and C. Soukoulis, "Effective medium theory of left-handed materials," *Physical review letters*, vol. 93, no. 10, p. 107402, 2004.

[8] R. Marqués, F. Medina, and R. Rafii-El-Idrissi, "Role of bianisotropy in negative permeability and left-handed metamaterials," *Physical Review B*, vol. 65, no. 14, p. 144440, 2002.

[9] R. Melik, E. Unal, N. K. Perkgoz, B. Santoni, D. Kamstock, C. Puttlitz, and H. V. Demir, "Nested metamaterials for wireless strain sensing," *IEEE Journal of Selected Topics in Quantum Electronics*, vol. 16, no. 2, p. 450, 2010.

[10] B. Ozbey, E. Unal, H. Ertugrul, O. Kurc, C. M. Puttlitz, V. B. Erturk, A. Altintas, and H. V. Demir, "Wireless displacement sensing enabled by metamaterial probes for remote structural health monitoring," *Sensors*, vol. 14, no. 1, p. 1691, 2014.

[11] R. W. Ziolkowski, P. Jin, and C.-C. Lin, "Metamaterial-inspired engineering of antennas," *Proceedings of the IEEE*, vol. 99, no. 10, p. 1720, 2011.

[12] E. Ekmekci and G. Turhan-Sayan, "Metamaterial sensor applications based on broadside-coupled srr and v-shaped resonator structures," in *Antennas and Propagation (APSURSI), 2011 IEEE International Symposium on*, p. 1170, IEEE, 2011.

[13] T. Driscoll, G. Andreev, D. Basov, S. Palit, S. Cho, N. Jokerst, and D. Smith, "Tuned permeability in terahertz split-ring resonators for devices and sensors," *Applied Physics Letters*, vol. 91, no. 6, p. 062511, 2007.

[14] H.-J. Lee and J.-G. Yook, "Biosensing using split-ring resonators at microwave regime," *Applied Physics Letters*, vol. 92, no. 25, p. 254103, 2008.

[15] H.-J. Lee, H.-S. Lee, K.-H. Yoo, and J.-G. Yook, "On the possibility of biosensors based on split ring resonators," in *Microwave Conference, 2008. EuMC 2008. 38th European*, p. 1222, IEEE, 2008.

[16] E. Cubukcu, S. Zhang, Y.-S. Park, G. Bartal, and X. Zhang, "Split ring resonator sensors for infrared detection of single molecular monolayers," *Applied Physics Letters*, vol. 95, no. 4, p. 043113, 2009.

[17] R. Melik, E. Unal, N. K. Perkgoz, C. Puttlitz, and H. V. Demir, "Metamaterial-based wireless strain sensors," *Applied Physics Letters*, vol. 95, no. 1, p. 011106, 2009.

[18] B. Ozbey, V. B. Erturk, H. V. Demir, A. Altintas, and O. Kurc, "A wireless passive sensing system for displacement/strain measurement in reinforced concrete members," *Sensors*, vol. 16, no. 4, p. 496, 2016.

[19] A. Alipour, E. Unal, S. Gokyar, and H. V. Demir, "Development of a distance-independent wireless passive rf resonator sensor and a new telemetric measurement technique for wireless strain monitoring," *Sensors and Actuators A: Physical*, vol. 255, p. 87, 2017.

[20] C. Mandel, M. Schüßler, and R. Jakoby, "A wireless passive strain sensor," in *Sensors, 2011 IEEE*, p. 207, IEEE, 2011.

[21] C. Mandel, B. Kubina, M. Schüßler, and R. Jakoby, "Passive chipless wireless sensor for two-dimensional displacement measurement," in *Microwave Conference (EuMC), 2011 41st European*, p. 79, IEEE, 2011.

[22] J. Naqui, M. Durán-Sindreu, and F. Martín, "Alignment and position sensors based on split ring resonators," *Sensors*, vol. 12, no. 9, p. 11790, 2012.

[23] A. K. Horestani, C. Fumeaux, S. F. Al-Sarawi, and D. Abbott, "Displacement sensor based on diamond-shaped tapered split ring resonator," *IEEE Sensors Journal*, vol. 13, no. 4, p. 1153, 2013.

[24] B. Ozbey, H. V. Demir, O. Kurc, V. B. Ertürk, and A. Altintas, "Wireless sensing in complex electromagnetic media: Construction materials and structural monitoring," *IEEE Sensors Journal*, vol. 15, no. 10, p. 5545, 2015.

[25] J. Naqui, M. Durán-Sindreu, and F. Martín, "Novel sensors based on the symmetry properties of split ring resonators (srrs)," *Sensors*, vol. 11, no. 8, p. 7545, 2011.

[26] J. Naqui and F. Martín, "Angular displacement and velocity sensors based on electric-lc (elc) loaded microstrip lines," *IEEE Sensors Journal*, vol. 14, no. 4, p. 939, 2014.

[27] J. Naqui, F. Martı, *et al.*, "Transmission lines loaded with bisymmetric resonators and their application to angular displacement and velocity sensors," *IEEE Transactions on Microwave Theory and Techniques*, vol. 61, no. 12, p. 4700, 2013.

[28] J. Mata-Contreras, C. Herrojo, and F. Martn, "Application of split ring resonator (srr) loaded transmission lines to the design of angular displacement and velocity sensors for space applications," *IEEE Transactions on Microwave Theory and Techniques*, vol. PP, no. 99, p. 1, 2017.

[29] C. Herrojo, F. Paredes, J. Mata-Contreras, S. Zuffanelli, and F. Martn, "Multistate multiresonator spectral signature barcodes implemented by means of s-shaped split ring resonators (s-srrs)," *IEEE Transactions on Microwave Theory and Techniques*, vol. PP, no. 99, p. 12, 2017.

[30] A. K. Horestani, D. Abbott, and C. Fumeaux, "Rotation sensor based on horn-shaped split ring resonator," *IEEE Sensors Journal*, vol. 13, no. 8, p. 3014, 2013.

[31] A. Ebrahimi, W. Withayachumnankul, S. F. Al-Sarawi, and D. Abbott, "Metamaterial-inspired rotation sensor with wide dynamic range," *IEEE Sensors Journal*, vol. 14, no. 8, p. 2609, 2014.

[32] W. Sun and W. J. Li, "Mems high-speed angular-position sensing system with rf wireless transmission," *Proc. SPIE*, vol. 4334, p. 244, 2001.

[33] H.-J. Sheng, W.-F. Liu, and M.-Y. Fu, "360-degree rotation sensor using a chirped fiber grating," *IEEE Photonics Technology Letters*, vol. 26, no. 2, p. 162, 2014.

[34] W. Yi-qun, L. Wei, and Z. Jia-lin, "A difference saw rotation sensor," *2006 IEEE International Conference on Information Acquisition*, p. 866, 2006.

[35] H. Tiersten, D. Stevens, and P. Das, "Acoustic surface wave accelerometer and rotation rate sensor," in *1980 Ultrasonics Symposium*, p. 692, IEEE, 1980.

[36] J. Scheuer and B. Z. Steinberg, "Coupled lasers rotation sensor (clars)," *Journal of Lightwave Technology*, vol. 26, no. 23, p. 3803, 2008.

[37] W. K. Burns, P. F. Liao, and P. Kelley, *Optical fiber rotation sensing*. Academic Press, 2012.

[38] G. Karapetyan, "Microwave gyroscope-novel rotation sensor," *arXiv preprint physics/0011014*, 2000.

[39] S. I. Latif, L. Shafai, and S. K. Sharma, "Bandwidth enhancement and size reduction of microstrip slot antennas," *IEEE Transactions on Antennas and Propagation*, vol. 53, no. 3, p. 994, 2005.

[40] A. Maleki Gargari, B. Ozbey, H. V. Demir, A. Altintas, U. Albostan, O. Kurc, and V. B. Ertürk, "A wireless metamaterial-inspired passive rotation sensor with an unprecedented submilliradian level of resolution," *in submission*, 2017.

[41] D. Vicari, *A Note on the Coefficient of Determination*. Dipartimento di statistica, probabilità e statistiche applicate, Università degli studi di Roma La Sapienza.. Ser. A, Ricerche, 1996.

[42] B. Ozbey, E. Unal, H. Ertugrul, O. Kurc, C. M. Puttlitz, V. B. Erturk, A. Altintas, and H. V. Demir, "Wireless displacement sensing enabled by metamaterial probes for remote structural health monitoring," *Sensors*, vol. 14, no. 1, p. 1691, 2014.

[43] U. Albostan and Ö. Kurç, "Application of 2D digital image correlation: Three points flexure test of reinforced concrete beam," *12th International Congress on Advances in Civil Engineering. Istanbul*, 2016.